# Erosion Study of Poly(ethylene tetrafluoroethylene) (Tefzel) by Hyperthermal Atomic Oxygen

**Michael L. Everett and Gar B. Hoflund***

*Department of Chemical Engineering, University of Florida, Gainesville, Florida 32611*

*Received March 10, 2004; Revised Manuscript Received May 23, 2004*

ABSTRACT: In this study the erosion of poly(ethylene tetrafluoroethylene) (ETFE) (Tefzel) by hyperthermal atomic oxygen (AO) has been examined using X-ray photoelectron spectroscopy (XPS). Initially, the Tefzel film had F/C and O/C atom ratios of 0.74 and 0.04, which decrease to 0.17 and 0.01, respectively, after a 2 h exposure to a flux of $2 \times 10^{15}$ atoms/(cm$^2$ s) AO with an average kinetic energy of 5 eV. The F/C atom ratio is further reduced to 0.02 with longer AO exposures, essentially producing a graphitic or amorphous carbon-like layer with a carbon content greater than 90 at. %. Longer AO exposures do not alter the composition of this layer significantly. Exposure of the AO-damaged surface to $O_2$ or air nearly doubles the oxygen content in the near-surface region. This is due to dissociative oxygen adsorption at reactive sites formed at the polymer surface during AO exposure. Further exposure to AO removes this chemisorbed oxygen. C−H bonds are important sites for attack during erosion by hyperthermal AO.

## Introduction

Polymers are attractive and desirable materials for use in space applications because they are lightweight and typically much easier to process using techniques such as extrusion, casting, and injection molding at relatively low temperatures compared to metals and ceramics. They also tend to be more flexible and offer a wide variety of choices from optically transparent to opaque, rubbery to stiff, and conducting to insulating. However, over the past two decades, it has been well established that polymers undergo severe degradation, resulting in reduced spacecraft lifetimes. These materials degrade because spacecraft surfaces are exposed to high fluxes of atomic oxygen (AO), bombardment by low- and high-energy charged particles, thermal cycling, and the full spectrum of solar radiation. AO is the main constituent of the atmosphere in low earth orbit (LEO). It is formed by dissociation of molecular oxygen by ultraviolet radiation from the sun, resulting in an AO concentration of approximately $10^8$ atoms/cm$^3$. The reverse reaction in which an oxygen molecule forms from AO does not have a high reaction rate because it requires a teratomic collision. The third atom is required to dissipate the energy released by formation of $O_2$. The actual flux of $\sim 10^{14}$ atoms/(cm$^2$ s) impinging on a spacecraft is high due to orbiting speeds of approximately 7.2 km/s. At these relative speeds thermal AO collides with a kinetic energy of ~4.5 eV.[1] These highly energetic collisions not only result in surface chemical reactions but can also lead to a pure physical sputtering of the surface atoms in the absence of any chemical changes. Many studies have been conducted in an effort to determine the mechanism of this degradation primarily caused by surface reactions with AO.[1−9] However, these studies have all been carried out after exposing these highly reactive surfaces to air prior to analysis, thus introducing artifacts that do not represent the true space environment. Recent studies have shown that exposure to air chemically alters the reactive surfaces formed during AO exposure.[10,11] It is, therefore, essential that analysis of polymers exposed to AO be carried out in situ to avoid artifacts induced by air exposure. An understanding of how AO alters polymer surfaces will aid in the development of new materials with acceptable erosion properties.

Recently, several polymer systems have been characterized in situ using X-ray photoelectron spectroscopy (XPS) before and after incremental exposures to the flux produced by an electron-stimulated desorption (ESD) AO source.[12−14] These studies have shown that polymers containing polyhedral oligomeric silsesquioxane (POSS) moieties rapidly form a passivating silica layer which serves as a protective barrier preventing further degradation of the underlying polymer with increased exposure to the AO flux. In this study a series of fluoropolymer films have been investigated in an effort to further understand AO-induced surface alterations of different polymer systems and to establish a basis for comparison in future POSS-fluorinated polymer studies. The polymers chosen for this study include Tedlar, poly(vinyl fluoride) (PVF), Tefzel, ethylene tetrafluoroethylene (ETFE), and Teflon, poly(tetrafluoroethylene) (PTFE), having fluorine-to-carbon ratios of 1:2, 1:1, and 2:1, respectively. High-density polyethylene (HDPE), which does not contain fluorine, was also examined. In this part of the study, long-time AO exposures of Tefzel have been examined.

Several studies have been conducted on the deterioration of fluorinated polymers retrieved from spacecraft subjected to the LEO environment. The outer layer of Teflon-fluorinated ethylene propylene (FEP) multilayer insulation on the Hubble space telescope (HST) was significantly cracked at the time of the second HST servicing mission, 6.8 years after it was launched into LEO.[15,16] Comparatively minor embrittlement and cracking were also observed in the FEP materials retrieved from solar-facing surfaces on the HST at the time of the first servicing mission (3.6 years of exposure). Furthermore, an increased deterioration of fluorinated polymers results from the synergistic effect of VUV radiation in the presence of AO.[17] Thin films of fluorinated polymers such as Teflon-FEP are used as the outer layer of multilayer thermal control insulation because of their

* Corresponding author: fax 352-392-9513, e-mail garho@hotmail.com.

10.1021/ma049515r CCC: $27.50 
Published on Web 07/09/2004

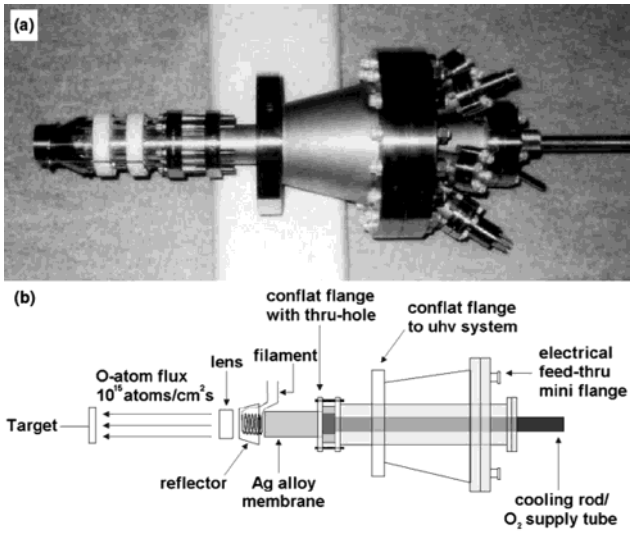


**Figure 1.** (a) Photograph of the atomic oxygen source and (b) schematic diagram of the atomic oxygen source.

superior optical properties, including low solar absorbency and high thermal reflectance. A metallized layer is applied to the backside in order to reflect incident sunlight.[15]

## Experimental Section

**O Atom Source Characteristics.** A photograph of the ESD AO source is shown in Figure 1a, and a schematic diagram illustrating the operational principles of the ESD AO source is shown in Figure 1b. Ultrahigh-purity molecular oxygen dissociatively adsorbs on the high-pressure (2 Torr) side of a thin metallic Ag-alloy membrane maintained at elevated temperature (∼400 °C) and permeates through the membrane to the UHV side. There the chemisorbed atoms are struck by a directed flux of primary electrons, which results in ESD of the O atoms forming a continuous flux. The primary electrons are produced by thermionic emission from a coiled hot filament supported around the perimeter of the membrane. An electron reflector (lens assembly) surrounds the filament. It produces a potential field, which creates a uniform flux of electrons over the membrane surface. These primary electrons have a kinetic energy of 1000 eV and provide two functions: ESD of the O atoms and heating of the membrane surface. Another lens is placed between the reflector and the sample for removal of all charged particles, including secondary electrons and small amounts of $O^+$ and $O^-$ ions produced during the ESD process.

Several processes have to function in series at sufficiently high rates for this system to work, including dissociative chemisorption of the molecular gas on the metal surface, permeation of atomic oxygen through the membrane, and formation of the neutral flux by ESD. Since these processes occur in series, the slowest one determines the magnitude of the AO flux. The sticking coefficient of $O_2$ on polycrystalline Ag (step 1) is fairly small (<0.001) so it is necessary to use a high pressure on the upstream side of the membrane. However, the permeation rate through the membrane is proportional to the reciprocal of the membrane thickness. This means that it is desirable to have a high pressure and a thin membrane, but this combination can lead to membrane failure. The ESD rate can be increased by increasing the primary electron current to the membrane, but this increases the temperature of the membrane and can result in evaporation of Ag, which is unacceptable.

The AO produced by this source has been shown to be hyperthermal (energies greater than 0.01−0.02 eV), but the neutral energy distribution has not been measured. Corallo et al.[18] have measured the energy distribution of O ions emitted by ESD from a Ag(110) surface and found that this distribution has a maximum of ∼5 eV and a full width at half-maximum of 3.6 eV. This ion energy distribution may set an upper bound for the neutral energy distribution because ESD neutrals are generally believed to be less energetic than ESD ions based on models of the ESD process. This point has been discussed often in the ESD literature but not actually demonstrated. Since neutral ESD species are difficult to detect, very few ESD studies of neutral species have appeared in the literature. The neutral atom flux has been detected by using a quadrupole mass spectrometer[19,20] in the appearance potential (AP) mode to allow the atoms to be distinguished from residual gases and background gas products formed by collisions of the neutrals with the walls of the UHV system. In this experiment the ion acceleration potential was set at 0.0 V. Calibration studies have demonstrated that the ions entering the quadrupole section must have a minimum kinetic energy of 2.0 eV to reach the detector so the ESD neutrals detected have a minimum energy of 2.0 eV. Therefore, the hyperthermal AO produced by this ESD source have energies greater than 2 eV but possibly less than the ion energy distribution. Furthermore, these mass spectrometric experiments have shown that the AO-to-$O^+$ ratio is about $10^8$ and that the $O^+$-to-$O^-$ ratio is about 100.

Several approaches have been used to measure the magnitude of the hyperthermal AO flux, and reasonable agreement was obtained between the various methods. The flux from the ESD AO source is approximately $2 \times 10^{15}$ atoms/(cm$^2$ s). One of the most reliable methods for flux determination is the measurement of a $ZrO_2$ film growth rate.[21] A Zr flux was generated by e-beam evaporation and the flux was calibrated using a quartz-crystal monitor. On the basis of the facts that stoichiometric $ZrO_2$ was produced and that no $O_2$ is present in the AO flux, the AO flux was calculated. By doubling the Zr flux, stoichiometric ZrO was grown.[22] The AO flux has also been determined by measuring the chemisorption rate of AO on polycrystalline Au using ion scattering spectroscopy.[23] The flux determined using this method is in excellent agreement with that determined using the oxide growth rate method.

**Surface Characterization.** An as-received E.I. du Pont Nemours & Co., Inc., Tefzel film was wiped with methanol and inserted into the UHV chamber (base pressure $<1.3 \times 10^{-10}$ Torr). XPS measurements were performed using a double-pass cylindrical mirror analyzer (DPCMA) (PHI model 25-270AR). XPS survey spectra were taken in the retarding mode with a pass energy of 50 eV, and high-resolution XPS spectra were taken with a pass energy of 25 eV using Mg Kα X-rays (PHI model 04-151 X-ray source). Data collection was accomplished using a computer interfaced, digital pulse-counting circuit[24] followed by smoothing with digital-filtering techniques.[25] The sample was tilted 30° off the axis of the DPCMA, and the DPCMA accepted electrons emitted into a cone 42.6 ± 6° off the DPCMA axis.

XPS spectra were first obtained from the as-entered, solvent-cleaned sample. The sample was then transferred into an adjoining UHV chamber that houses the ESD AO source via a magnetically coupled rotary/linear manipulator. There the surface was exposed to the hyperthermal AO flux and reexamined after various exposure times. The samples were not exposed to air after the AO exposures and before collecting XPS data. However, after the AO exposures the surface was exposed to $O_2$ to determine how this would affect the AO-exposed surfaces. The approximate normal distance between the sample face and source in this study was 15 cm, at which distance the flux was about $2.0 \times 10^{15}$ atoms/(cm$^2$ s) for the instrument settings used. The sample was maintained at room temperature during the AO exposures with a temperature increase to about 50 °C due to exposure to the X-ray source during XPS data collection. The substrate temperature was determined using a chromel−alumel thermocouple. Polymer structural repeat units, F-to-C ratios, and reference XPS binding energies (BEs) used in this study are given in Table 1.

## Results and Discussion

XPS survey spectra obtained from the as-entered Tefzel before and after 2 h of AO exposure are shown

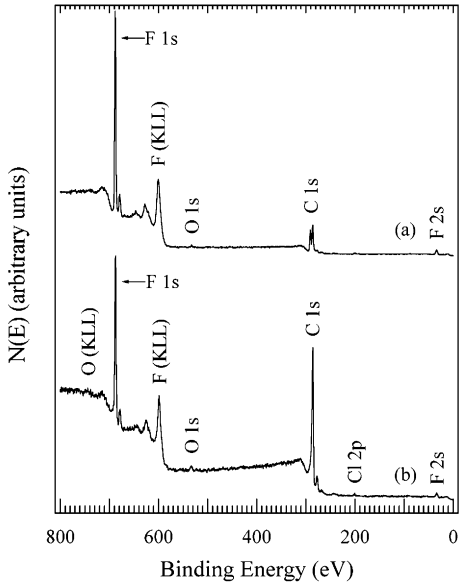


**Figure 2.** XPS survey spectra obtained from Tefzel (a) as entered and (b) after 2 h exposure to AO.

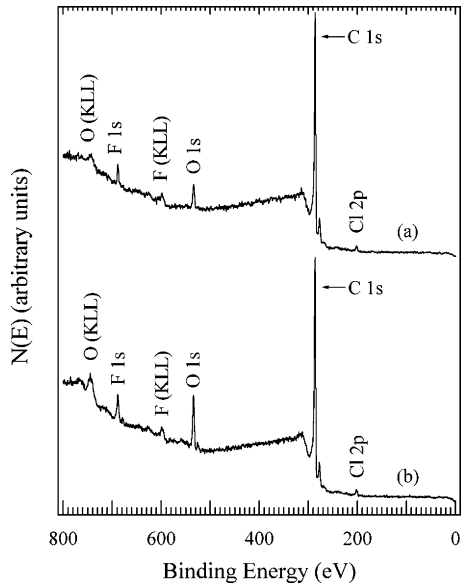


**Figure 3.** XPS survey spectra obtained from Tefzel (a) after 24 h exposure to AO and (b) after 20 min exposure to $O_2$ at 150 Torr and room temperature.

**Table 1. Polymer Name, XPS Binding Energies, F/C Ratio, and Structure**

| | binding energy (eV) | | | |
|---|---|---|---|---|
| | C 1s | | | |
| polymer | 1 | 2 | F 1s | F:C |
| Tefzel, poly(ethylene tetrafluoroethylene) $[-CH_2-CH_2-CF_2-CF_2-]_n$ | 286.44 | 290.90 | 688.15 | 1:1 |

**Table 2. Near-Surface Compositions of Tefzel after Various Treatments (at. %)**

| | F | O | C | F/C | O/C |
|---|---|---|---|---|---|
| as entered | 41.5 | 2.3 | 56.2 | 0.74 | 0.04 |
| AO 2 h | 14.5 | 0.7 | 84.8 | 0.17 | 0.01 |
| AO 24 h | 1.9 | 3.5 | 94.7 | 0.02 | 0.04 |
| $O_2$ 20 min | 3.7 | 7.2 | 89.1 | 0.04 | 0.08 |
| AO 25 h | 1.7 | 6.8 | 91.5 | 0.02 | 0.07 |
| AO 28 h | 1.2 | 4.9 | 93.9 | 0.01 | 0.05 |

in parts a and b of Figure 2, respectively. The predominant peaks apparent in these spectra include the C 1s, O 1s, F 1s, F Auger (KLL), and F 2s. A small C1 2p peak is also present near 200 eV. Significant changes in relative peak heights are observed for the C and F features following the AO exposure. Estimates of the near-surface compositions have been made from the peak areas in the high-resolution spectra using published atomic sensitivity factors[26] with the assumption of a homogeneous surface region. XPS probes the near-surface region of the sample and yields a weighted average composition with the atomic layers near the surface being weighted more heavily since the photoemitted electrons from these layers have a lower probability of scattering inelastically. The sampling depth is ~4−6 nm, and ~10% of the signal originates from the outermost atomic layer.[27] This near-surface region is nonhomogeneous because the AO reacts most strongly with the outermost few atomic layers. Therefore, the region that reacts to the greatest extent with AO also makes the largest contribution to the XPS signal. This fact implies that XPS is an excellent technique for studying AO erosion of spacecraft materials. Even though the distribution functions involving the depth of chemical reactions in the near-surface region and the XPS determination of the weighted average composition of the near-surface region are complex, the compositional values provide a trend which is indicative of the chemical alterations occurring during AO exposure.

The compositions determined using the homogeneous assumption are shown in Table 2 before and after various exposures to AO and $O_2$. The F/C atom ratio obtained from the as-entered sample is 0.74, which is lower than the stoichiometric value of 1.0. The near-surface region also contains about 2.3 at. % of O, giving an O/C atom ratio of 0.04. The source of this surface O is not known. It may have accumulated during preparation of the Tefzel, and it may be present in the bulk of the polymer. It possibly is due to an oxygen-containing termonomer such as terfluoropropyl vinyl ether, which may have been added to Tefzel to improve cracking resistance.

After a 2 h AO exposure (survey spectrum shown in Figure 2b), the F/C atom ratio is decreased from 0.74 to 0.17, and the O/C atom ratio is significantly reduced from 0.04 to 0.01. Furthermore, the chemical composition of the outermost 30−50 Å consists of 84.8 at. % C. Stoichiometric Tefzel consists of equal atomic percents of C, F, and H. Unfortunately, XPS is relatively insensitive to H because it has no core level electrons. Therefore, H is not measured although it is certainly present at least initially. Both AO and H are highly reactive. AO most likely reacts with H in the near-surface region to form $H_2O$, which desorbs leaving a carbonaceous layer. The structure of this carbonaceous layer has not been determined and most likely is quite complex. It may be partially graphitic, and it may contain amorphous regions as well as double and triple unsaturated bonds. It may be considered to be a charcoal-like layer produced after just 2 h of AO exposure. All further experiments are carried out on this layer and not on a Tefzel layer. The XPS spectrum obtained after a 24 h AO exposure (Figure 3a) differs significantly from the spectrum obtained after the 2 h AO exposure in that the F 1s peak is much smaller relative to the C 1s peak and the O 1s peak size is increased. The latter is probably due to adsorption of O at unsaturated bonds formed by further erosion of the C-rich layer. According

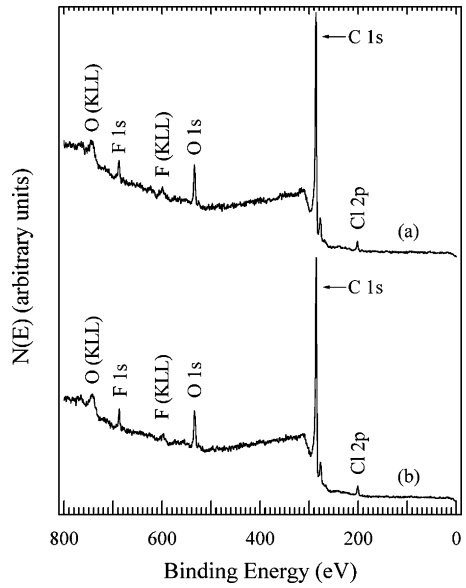


**Figure 4.** XPS survey spectra obtained from Tefzel (a) after 25 h exposure to AO and (b) after 28 h exposure to AO.

to the compositional data in Table 2, the C content is increased to 94.7 at. %, the O content is increased to 3.5 at. %, and the F content is decreased from 14.5 to 1.9 at. %. This layer is considerably more carbonaceous than that obtained after the 2 h AO exposure.

After exposure of this surface to $O_2$ at 150 Torr and room temperature for 20 min, the XPS O 1s peak is clearly increased (Figure 3b). The compositional data in Table 2 indicate that the O/C atom ratio is increased from 0.04 to 0.08. This increase is due to dissociative chemisorption of $O_2$ at reactive sites formed during the erosion process. The amount of $O_2$ adsorbed provides a measure of the concentration of reactive sites formed during AO exposure. A charcoal or graphite surface would not adsorb any $O_2$ under these exposure conditions. The $O_2$-exposed surface was then exposed to AO for 1 h (25 h total) and another 3 h (28 h total). The resulting XPS survey spectra are shown in parts a and b of Figure 4, respectively. The O 1s peak is slightly decreased in size relative to the C 1s peak. This is supported by the compositional information in Table 2 in which the O/C atom ratio decreases from 0.08 to 0.07. Furthermore, the F/C atom ratio decreases from 0.04 to 0.02. After another 3 h of AO exposure, the survey spectrum shown in Figure 4b was obtained. From Table 2 the F/C and O/C atom ratios are 0.01 and 0.05, respectively. These are quite similar to the values obtained after the 24 h AO exposure. The composition of this surface is probably similar to the steady-state composition during the AO process. Since the C concentration is very large, the formation of CO and/or $CO_2$ is the slow step in the erosion process. Surface F is most likely removed by a physical sputtering process by the hyperthermal AO while surface O may be removed by either physical sputtering or chemical reaction to form $O_2$ or both at different rates.

The high-resolution XPS C 1s, O 1s, and F 1s features are shown in parts A, B, and C of Figure 5, respectively. The C 1s feature obtained from the as-entered Tefzel (Figure 5Aa) consists of two peaks with maxima at 286.4 and 291.0 eV. This is consistent with reference spectra obtained from Tefzel.[28] The feature at 286.4 eV is assigned as due to C bonded as $-CH_2-$, and the feature at 291.0 eV is assigned to C bonded as $-CF_2-$. The

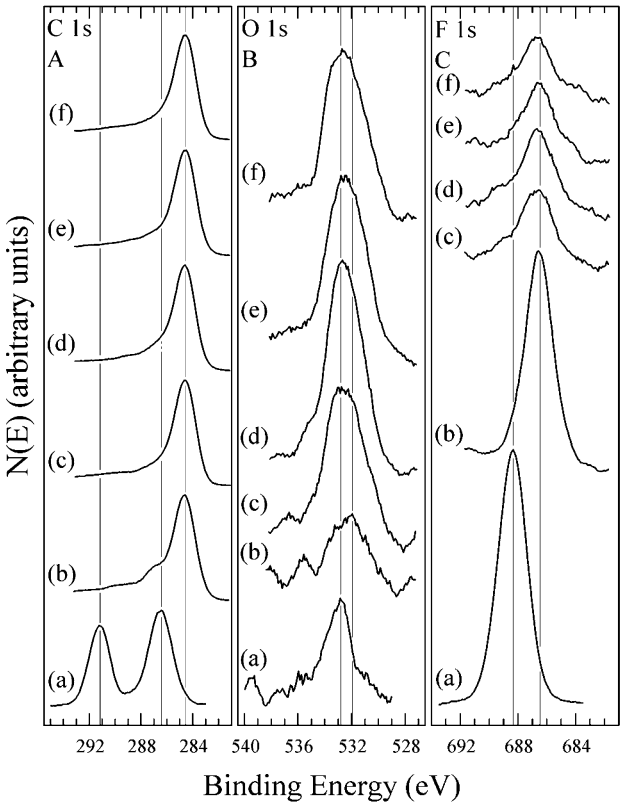


**Figure 5.** High-resolution (A) C 1s, (B) O 1s, and (C) F 1s spectra obtained (a) from the as-entered Tefzel, (b) after a 2 h AO exposure, (c) after a 24 h AO exposure, (d) after a 20 min exposure to $O_2$ at atmospheric pressure and room temperature, (e) after a 25 h exposure to AO, and (f) after a 28 h exposure to AO.

peaks should be the same size since these two types of C are present in stoichiometric Tefzel in equal amounts, and this is the case in the reference spectra.[28] Stoichiometric Tefzel also contains no O whereas the as-entered sample in this study contained about 2.3 at. %. This O is most likely bonded in the near-surface region as $-CH(OH)-$ groups, which have a C 1s binding energy (BE) of about 286.5 eV.[28] The presence of these groups adds structure to the lower BE feature, thereby increasing its intensity and broadening it to the low BE side. It seems reasonable that $-CH(OH)-$ groups would have a C 1s BE between the two peaks observed in Figure 5Aa. Since features are not apparent at these BEs, $-CF(OH)-$ species are not present. The O 1s feature obtained from the as-entered Tefzel (Figure 5Ba) is consistent with the assertions above in that it is small and symmetrical. This latter point indicates the presence of only one chemical state of O. Furthermore, the BE of this peak is 532.9 eV, which is the median of the narrow range ($\Delta E = 0.35$ eV) reported by Beamson and Briggs[28] for the proposed species. The F 1s peak is also symmetrical with a BE of 688.3 eV. This is characteristic of F in $-CHF-$ groups.[28]

The C 1s, O 1s, and F 1s spectra obtained after the 2 h AO exposure are shown in parts Ab, Bb, and Cb of Figure 5, respectively. The C 1s feature consists of a predominant symmetrical peak with a BE of 284.6 eV, which is characteristic of a graphitic or an amorphous charcoal-like C film. This is reasonable since the near-surface region contains 84.8 at. % C, 14.5 at. % F, and 0.7 at. % O (Table 2). The C 1s feature also contains a shoulder on the high-BE side of the predominant

feature. This shoulder is due to carbon which is bonded to the remaining F. Since the BE is lower than that of C bonded to two fluorines, this shoulder is probably due to C bonded to just one F species. The other F is most likely removed by physical sputtering. Another very slight shoulder is apparent at 289.6 eV. This is probably due to C, which is still bonded to two fluorines. By comparing parts Ba and Bb of Figure 5, it is apparent that the chemical nature of O in the near-surface region is changed by the 2 h AO exposure. This exposure decreases the O concentration from 2.3 to 0.7 at. %. The chemical state at 532.9 eV is reduced in intensity while chemical states with BEs in the range from 530.6 to 532.3 eV are formed. The chemical nature of these O species is not known, but they may be C−O−C, C−OH, or C═O groups.[28] The fact that these AO-exposed surfaces are quite damaged makes species assignment very difficult. The F 1s peak is significantly decreased in size (the F/C atom ratio is reduced from 0.74 to 0.17), and the BE of the predominant feature is shifted to 686.5 eV and broadened toward lower BEs. These values are lower than any reported F 1s values for organic materials containing F. One possibility is that the F may be interacting with radical species capable of donating electrons to the F, thereby lowering the F 1s BE.

After the 24 h AO exposure, the predominant peak in the C 1s feature remains unchanged, but the higher BE shoulders are significantly reduced in intensity. This is consistent with the compositional information since these shoulders are due to bonding with O or F. The F content is reduced from 14.5 to 1.9 at. % while the O content is increased from 0.7 to 3.5 at. %. This increase in O content is most likely due to bonding of AO with carbon-centered radicals remaining after F removal. At least four chemical states of oxygen are apparent after the 24 h AO exposure (Figure 5Bc). The corresponding F 1s feature (Figure 5Cc) is small and broad, indicating that F is bonded in many chemical environments in this heavily damaged near-surface region.

After the $O_2$ exposure the C 1s feature (Figure 5Ad) is broadened slightly on the high-BE side. The corresponding O 1s feature (Figure 5Bd) is fairly symmetrical around the predominant peak with a BE of 532.7 eV. This is quite likely due to a C═O species formed by dissociative chemisorption of $O_2$ at reactive C sites. The F 1s peak (Figure 5Cd) is narrower after the $O_2$ exposure possibly due to saturation of the reactive species formed during AO exposure.

After another 1 h and then 3 h of AO exposure, only a few small changes are observed in the high-resolution spectra. The small shoulder on the high-BE side of the C 1s peak (Figure 5Ae,Af) is more similar to that obtained after the 24 h AO exposure (Figure 5Ac). The O 1s feature (Figure 5Be,Bf) is broadened and is quite similar to that obtained after the 24 h AO exposure (Figure 5Bc). The F 1s peak becomes quite small with further AO exposure but retains its narrow, symmetrical nature.

These spectra along with the compositional data shown in Table 2 indicate that the surface produced by the 24-AO exposure is the steady-state surface formed during AO erosion of Tefzel. The fact that the C content of the near-surface region is about 95 at. % indicates that removal of C from the surface either by reaction with AO to form CO and/or $CO_2$ or by physical sputtering by the hyperthermal AO is the slow step in the erosion process. The F is removed rapidly, and the H most likely is removed rapidly as well since it is very reactive toward AO. Oxygen in the near-surface region apparently is not removed as fast as F.

**Table 3. Near-Surface Compositions of Tedlar after Various Treatments (at. %)**

| | F | O | C | F/C | O/C |
|---|---|---|---|---|---|
| as entered | 29.0 | 7.2 | 63.7 | 0.45 | 0.11 |
| AO 2 h | 1.7 | 4.0 | 94.2 | 0.018 | 0.04 |
| AO 24 h | 2.0 | 6.3 | 91.7 | 0.022 | 0.07 |
| $O_2$ 20 min | 1.1 | 10.4 | 88.5 | 0.012 | 0.12 |
| AO 25 h | 1.3 | 7.0 | 91.7 | 0.014 | 0.08 |
| AO 28 h | 1.7 | 6.7 | 91.6 | 0.018 | 0.07 |

**Table 4. Near-Surface Compositions of TFE Teflon after Various Treatments (at. %)**

| | F | O | C | F/C | O/C |
|---|---|---|---|---|---|
| as entered | 62.4 | 0.0 | 37.6 | 1.66 | 0.0 |
| AO 2 h | 53.6 | 0.0 | 46.4 | 1.15 | 0.0 |
| AO 24 h | 47.4 | 0.0 | 52.6 | 0.90 | 0.0 |
| $O_2$ 20 min | 46.8 | 0.8 | 52.4 | 0.90 | 0.015 |
| AO 25 h | 44.9 | 0.1 | 55.0 | 0.81 | 0.002 |
| AO 28 h | 45.2 | 0.0 | 54.8 | 0.82 | 0.0 |

Similar AO exposure studies have been carried out on poly(vinyl fluoride) (PVF) $(CHF-CH_2)_n$ (Tedlar) and poly(tetrafluoroethylene) (PTFE) $(CF_2-CF_2)_n$ (TFE Teflon) and the XPS compositional results corresponding to Table 2 for Tefzel are shown in Tables 3 and 4, respectively. The F content of the near-surface region decreases very rapidly for Tedlar, less rapidly for Tefzel, and relatively slowly for TFE Teflon with increasing AO fluence. This behavior correlates with the hydrogen content of these polymers. Tedlar is 50 at. % H, Tefzel is 33.3 at. % H, and Teflon is 0 at. % H. This information suggests that H atoms, i.e., H−C bonds, provide an attack point for AO possibly through formation of HF, which desorbs. After the surface structure is damaged, the F is susceptible to removal by AO. Since TFE Teflon does not contain H, the F is more difficult to remove. Furthermore, the C removal rate by AO is not much slower than the F removal rate so the F/C atom ratio only decreases from 1.66 to about 0.82 for the steady-state surface composition. This is quite different than Tedlar, where the F/C atom ratio drops from 0.45 to 0.01, and Tefzel, where the F/C atom ratio drops from 0.74 to 0.01. The steady-state compositions of Tedlar and Tefzel are nearly identical, containing 91.7 and 94.7 at. % C, respectively, while that for TFE Teflon is very different, containing only 52.6 at. % C. The reactions of the steady-state AO eroded surfaces with $O_2$ are also quite different. The O contents of both Tedlar and Tefzel are significantly increased after the $O_2$ exposure (O/C atom ratios increase from 0.07 to 0.12 for Tedlar and from 0.04 to 0.08 for Tefzel) while that for TFE Teflon only increases from 0.0 to 0.015. Again, this behavior correlates with the initial H content of the polymer. Polymers containing more H initially form more damage-laden films during AO exposure which adsorb more $O_2$.

## Summary

In this study a Tefzel film has been exposed to a flux of $2 \times 10^{15}$ atoms/(cm$^2$ s) of 5 eV AO for various times, and the chemical alterations at the surface have been monitored using XPS. After a 2 h exposure, the F/C and O/C atom ratios decrease from 0.74 and 0.04 to 0.17 and 0.01, respectively. Most of the F is removed, the O content is decreased from 2.3 to 0.7 at. %, and the C

content is increased from 56.2 to 84.8 at. %. A longer exposure of 24 h results in a further decrease of the F/C atom ratio to 0.02. This AO exposure transforms the near-surface region of Tedlar into a carbonaceous layer (94.7 at. % C), which may be graphitic or amorphous according to the high-resolution XPS data. This surface is the steady-state surface formed during the AO erosion of Tefzel since longer AO exposures do not significantly alter the chemical composition or nature of the carbonaceous film. This film is attacked chemically by AO to form CO and/or $CO_2$, resulting in erosion, but the erosion rate has not been determined in this study. On the basis of the XPS data, the thickness of the carbonaceous film is at least 4 nm. The fact that this surface consists mostly of C indicates that reaction of C with AO is the slow step in the erosion process. Comparison of the AO erosion data of Tefzel with similar data taken from Tedlar and TFE Teflon indicate that C−H bonds are sites that are highly susceptible to attack by AO.

Exposure of the AO-exposed carbonaceous film to $O_2$ increases the oxygen content of the near-surface region by a factor of about 2. The oxygen adsorbs at reactive sites formed during AO exposure. These reactive sites most likely do not cross-bond due to geometrical bond constraints. The amount of $O_2$ that chemisorbs provides a measure of the concentration of these reactive sites in the near-surface region. Further exposure to AO removes this chemisorbed oxygen to the level prior to the $O_2$ or air exposure.

**Acknowledgment.** Support for this research was received from the AFOSR through Grant F49620-01-0338.

## References and Notes

(1) Gindulyte, A.; Massa, L.; Banks, B. A.; Miller, S. K. R. *J. Phys. Chem. A* **2002,** *106,* 5463.
(2) Koontz, S. L.; Leger, L. J.; Visentine, J. T.; Hunton, D. E.; Cross, J. B.; Hakes, C. L. *J. Spacecraft Rockets* **1995**, *32,* 483.
(3) Tennyson, R. C. *Can. J. Phys.* **1991**, *69,* 1190.
(4) Koontz, S. L.; Leger, L. J.; Rickman, S. L.; Hakes, C. L.; Bui, D. T.; Hunton, D. E.; Cross, J. B. *J. Spacecraft Rockets* **1995**, *32,* 475.
(5) Reddy, M. R. *J. Mater. Sci.* **1995,** *30,* 281.
(6) Packirisamy, S.; Schwam, D.; Litt, M. H. *J. Mater. Sci.* **1995,** *30,* 308.
(7) Reddy, M. R.; Srinivasamurthy, N.; Agrawal, B. L. *Eur. Space Agency J.* **1992,** *16,* 193.
(8) de Groh, K. K.; Banks, B. A. *J. Spacecraft Rockets* **1994**, *31,* 656.
(9) Leger, L. J.; Visentine, J. T. *J. Spacecraft Rockets* **1986,** *23,* 505.
(10) Grossman, E.; Lifshitz, Y.; Wolan, J. T.; Mount, C. K.; Hoflund, G. B. *J. Spacecraft Rockets* **1999,** *36,* 75.
(11) Wolan, J. T.; Hoflund, G. B. *J. Vac. Sci. Technol. A* **1999,** *17,* 662.
(12) Gonzalez, R. I.; Phillips, S. H.; Hoflund, G. B. *J. Spacecraft Rockets* **2000,** *37,* 463.
(13) Phillips, S. H.; Hoflund, G. B.; Gonzalez, R. I. *Proc. 45th Int. SAMPE Symp.* **2000**, *45,* 1921.
(14) Hoflund, G. B.; Gonzalez, R. I.; Phillips, S. H. *J. Adhes. Sci. Technol.* **2001,** *15,* 1199.
(15) DeGroh, K. K.; Gaier, J. R.; Espe, M. P.; Cato, D. R.; Sutter, J. K.; Scheiman, D. A. *High Perform. Polym.* **2000,** *12,* 83.
(16) Dever, J. A.; DeGroh, K. K.; Banks, B. A.; Townsend, J. A.; Barth, J. L.; Thomson, S.; Gregory, T.; Savage, W *High Perform. Polym.* **2000,** *12,* 125.
(17) Rasoul, F. A.; Hill, D. J. T.; Forsythe, J. S.; O'Donnell, J. H.; George, G. A.; Pomery, P. J.; Young, P. R.; Connell, J. W. *J. Appl. Polym. Sci.* **1995,** *58,* 1857.
(18) Corallo, G. R.; Hoflund, G. B.; Outlaw, R. A. *Surf. Interface Anal.* **1988**, *12,* 185.
(19) Davidson, M. R.; Hoflund, G. B.; Outlaw, R. A. *Surf. Sci.* **1993**, *281,* 111.
(20) Outlaw, R. A.; Hoflund, G. B.; Corallo, G. R. *Appl. Surf. Sci.* **1987,** *28,* 23.
(21) Wisotzki, E.; Balogh, A. G.; Hahn, H.; Wolan, J. T.; Hoflund, G. B. *J. Vac. Sci. Technol. A* **1999,** *17,* 14.
(22) Wisotzki, E.; Hahn, H.; Hoflund, G. B. In *Trends and New Applications of Thin Films;* Hoffman, H., Ed.; Trans Tech Publications Ltd.: Switzerland, 1998; Vol. 181, pp 277−278.
(23) Davidson, M. R.; Hoflund, G. B.; Outlaw, R. A. *J. Vac. Sci. Technol. A* **1993,** *11,* 264.
(24) Gilbert, R. E.; Cox, D. F.; Hoflund, G. B. *Rev. Sci. Instrum.* **1982**, *53,* 1281.
(25) Savitzky, A.; Golay, M. J. E. *Anal. Chem.* **1964**, *36,* 1627.
(26) *Handbook of X-ray Photoelectron Spectroscopy*; Wagner, C. D., Riggs, W. M., Davis, L. E., Moulder, J. F., Muilenberg, G. E., Eds.; Perkin-Elmer Corp.: Eden Prairie, MN, 1979.
(27) Hoflund, G. B. In *Handbook of Surface and Interface Analysis: Methods in Problem Solving*; Rivière, J. C., Myhra, S., Eds.; Marcel Dekker: New York, 1998; pp 57−158.
(28) *High-Resolution XPS of Organic Polymers: The Scienta ESCA300 Database;* Beamson, G., Briggs, D., Eds.; Wiley: Chichester, 1992; pp 54, 226−236.

MA049515R